2010

Direct simulation Monte Carlo modeling of e-beam metal deposition

A Venkattraman
Purdue University

Alina A. Alexeenko
Purdue University - Main Campus, alexeenk@purdue.edu

Recommended Citation
Venkattraman, A and Alexeenko, Alina A., "Direct simulation Monte Carlo modeling of e-beam metal deposition" (2010). *School of Aeronautics and Astronautics Faculty Publications.* Paper 39.
http://dx.doi.org/10.1116/1.3386592

Direct simulation Monte Carlo modeling of e-beam metal deposition

A. Venkattraman and A. A. Alexeenko[a)]
School of Aeronautics and Astronautics, Purdue University, West Lafayette, Indiana 47907

(Received 4 November 2009; accepted 22 March 2010; published 29 June 2010)

Three-dimensional direct simulation Monte Carlo (DSMC) method is applied here to model the electron-beam physical vapor deposition of copper thin films. Various molecular models for copper-copper interactions have been considered and a suitable molecular model has been determined based on comparisons of dimensional mass fluxes obtained from simulations and previous experiments. The variable hard sphere model that is determined for atomic copper vapor can be used in DSMC simulations for design and analysis of vacuum deposition systems, allowing for accurate prediction of growth rates, uniformity, and microstructure. © *2010 American Vacuum Society.* [DOI: 10.1116/1.3386592]

I. INTRODUCTION

The vacuum processes for fabrication of thin-film materials play an increasingly important role in a variety of technologies. In the manufacture of optics and electronics, thin films of insulators, semiconductors and conductors form integrated circuits.[1] In the fabrication of microelectromechanical systems (MEMS) such as gyroscopes, rf switches, and resonators, layers of metals are often deposited under vacuum conditions.[2] Additionally, vacuum depositions represent a major element of bottom-up nanofabrication technologies.[3]

The deposition of thin films can be performed using various techniques including electron-beam assisted physical vapor deposition (EBPVD),[4] molecular beam epitaxy,[5] chemical vapor deposition,[6] and sputtering of particles by energetic ion bombardment.[7] Among these methods, the EBPVD is widely used due to the high deposition rates that can be attained at relatively low temperatures.[8,9] The EBPVD technique is based on the use of high-energy electron beams to assist in evaporation of metals, those vapors are then being expanded into vacuum and deposited on substrates.

The deposition of metal thin films using techniques listed above typically occurs at extreme temperatures and under high-vacuum requirements. The energy use during vacuum depositions scales inversely proportional to pressure and is a key factor in the overall environmental and economic costs of a thin-film manufacturing process.[10] As such techniques become more widely used, especially in the emerging nano- and microtechnologies, the application of modeling in the analysis and design of deposition systems and processes acquires a larger significance.

Modeling of vacuum deposition requires consideration of complex physical phenomena in the vapor phase such as the formation of supersonic vapor jets. Such high-velocity vapor flow increases the reactant kinetic energy and enhances the surface reaction probability on the substrate. A description of the vapor flow based on nonequilibrium kinetic theory of gases is required to predict the properties of the rapidly expanding flow, resultant spatial variation of the deposition rate, incidence angle, and energy. At low deposition rates, the flow is close to free-molecular and the Knudsen's cosine law[11] provides a good estimate of the growth rate. However, as the deposition rate is increased such that the resulting flow is in the transition regime of rarefied gas dynamics, the cosine law is no longer valid and a detailed modeling is required. The direct simulation Monte Carlo (DSMC) method[12] is *de facto* the most powerful numerical approach for solution of gas kinetic problems and can be used to simulate vapor flows expanding into vacuum from sources of complex geometries encountered in deposition systems.

Accurate modeling of vapor flows using the DSMC method for high deposition rates requires the specification of a molecular collision model for the vapor of interest. Such collision models are usually based on the measurements of transport properties such as coefficient of viscosity or thermal conductivity of the gas phase of a substance. However, such measurements of bulk transport coefficients are difficult to perform for non-volatile materials such as metal vapors. The main goal of this study is to evaluate various molecular models for metal vapors and determine a suitable model for DSMC simulations of thin-film vacuum deposition processes.

There have been a number of studies on modeling and experiments of thin-film depositions of various materials, including metals. Chen *et al.*[13–15] have applied DSMC simulations to model deposition of silicon thin films using supersonic molecular beams from different types of sources. Balakrishnan *et al.*[16] performed simulations of vapor transport in electron-beam deposition of titanium and Fan *et al.* considered the same for yttrium.[17] Sahu *et al.*[18] and Thakur *et al.*[19] carried out a series of experiments using the EBPVD technique for the deposition of copper. The published results contain experimental flux measurements of copper vapor for both axisymmetric sources and two-dimensional slit sources of various aspect ratios. However, there have been a relatively small number of published studies comparing the experimental data for metal deposition with simulations.

The majority of numerical simulations[20,21] performed using the DSMC technique for applications involving copper vapor have the hard sphere (HS) molecular model which

[a)]Electronic mail: alexeenk@purdue.edu

gives a square-root dependence of viscosity on temperature. Mukherjee *et al.*[21] have compared their simulation results with EBPVD experimental data. Such a comparison was performed between the nondimensional density values at the collector plate location obtained using DSMC simulations with the nondimensional mass flux, nondimensionalized with respect to the maximum value of mass flux, obtained from measurements. In fact, such nondimensional quantities will depend only on a similarity parameter, which in this case is the Knudsen number Kn defined as the ratio of the mean free path of the molecules, λ, to the characteristic length scale L,

$$\mathrm{Kn} = \frac{\lambda}{L}. \tag{1}$$

As will be shown in Sec. IV, two depositions with significantly different mass fluxes can have the same nondimensional mass flux profiles if they correspond to the same Kn conditions. The Knudsen number in turn depends on the molecular model parameters, which are not well established for metal vapors (e.g., copper). One of the objectives of this work is to formulate a molecular model for interaction of atomic copper suitable for use in the DSMC simulations of vacuum deposition systems.

The remainder of the article is organized as follows. Section II briefly explains the molecular models relevant to this work. Section III describes the flow conditions providing details of the computational domain and the experimental setup and also summarizes the DSMC simulation parameters used. Section IV presents the results and discussion with Sec. V reserved for conclusions.

II. MOLECULAR MODEL FOR METAL VAPORS

As mentioned earlier, the molecular model used to simulate the interaction between molecules is an important input in DSMC simulations. The general behavior of the interaction between neutral molecules can be summarized as negligible at large distances, weakly attractive at intermediate distances, and strongly repulsive at very small distances. Molecular models that are commonly used in DSMC simulations neglect the attractive component of the force. The simplest molecular model that is used in DSMC simulations is the HS model[12] which requires the specification of a reference diameter (d_{ref}) and a reference temperature (T_{ref}). The variation in viscosity as a function of temperature, for the HS model, can be obtained as

$$\mu = \mu_{\mathrm{ref}} \sqrt{\frac{T}{T_{\mathrm{ref}}}}. \tag{2}$$

The $\sqrt{T}$ variation in viscosity for all gases is viewed as the major disadvantage of the HS model which lead to the formulation of the variable hard sphere (VHS) model.[12] The VHS model is one of the models that is widely used due to its combination of simplicity and accuracy. It requires the specification of the reference molecular diameter (d_{ref}), viscosity-temperature exponent (ω), and a reference temperature (T_{ref}). The major difference between the HS and the VHS models is the fact that the diameter of the VHS model is a function of the relative velocities between the colliding molecules, unlike the HS model which has a constant diameter. The parameters for the VHS model are usually obtained from viscosity or thermal conductivity experimental data. However, such data are not easily available for metal vapors which do not exist in the gaseous state at room temperatures.

The mean free path λ for the VHS model is given by[12]

$$\lambda = \frac{1}{\sqrt{2}\pi n d_{\mathrm{ref}}^2 (T/T_{\mathrm{ref}})^{\alpha}}, \tag{3}$$

where $\alpha = \omega - 0.5$ and n is the number density of the vapor. The hard sphere model corresponds to $\omega = 0.5$ or $\alpha = 0.0$.

The variation in viscosity μ as a function of temperature for a VHS model is given by[12]

$$\mu = \mu_{\mathrm{ref}} \left(\frac{T}{T_{\mathrm{ref}}} \right)^{\omega}, \tag{4}$$

where μ_{ref} is the viscosity at the reference temperature T_{ref}.

The most widely used model that accounts for the attractive component of the force between molecules is the Lennard-Jones potential model.[22] The Lennard-Jones potential describes intermolecular interaction in the following form:

$$U = 4\epsilon \left[\left(\frac{\sigma}{r} \right)^{12} - \left(\frac{\sigma}{r} \right)^{6} \right], \tag{5}$$

where U is the potential energy, ϵ the depth of the potential well, and σ the distance at which the intermolecular potential is zero. The sixth power in the first term that characterizes the repulsion between molecules corresponds to electrostatic dipole-dipole interaction and hence leads to a more realistic interaction potential.

For copper-copper interaction, parameters of Lennard-Jones (LJ) potential are reported in Ref. 23 as

$$\sigma = 2.277 \times 10^{-10} \ \mathrm{m},$$

$$\epsilon = 0.415 \ \mathrm{eV}.$$

These values of the LJ potential parameters were extracted from experimental data on cohesive energy at room temperatures. Bird *et al.*[24] provided empirical correlations for the LJ potential parameters as functions of the molar volume and the normal boiling temperature,

$$\frac{\epsilon}{k} = 1.15 T_b, \tag{6}$$

$$\sigma = 1.166 V_{b,\mathrm{liq}}^{1/3}, \tag{7}$$

where k is the Boltzmann constant, ϵ/k is in units of Kelvin, σ is in Angstrom units, T_b is the boiling temperature in Kelvin, and $V_{b,\mathrm{liq}}$ is the molar volume in $\mathrm{cm}^3/\mathrm{mol}$. Using the relevant parameters for copper as $T_b = 2835$ K and $V_{b,\mathrm{liq}} = 7.11 \ \mathrm{cm}^3/\mathrm{mol}$, we get the following LJ parameters:

$$\sigma = 2.242 \times 10^{-10} \ \mathrm{m},$$

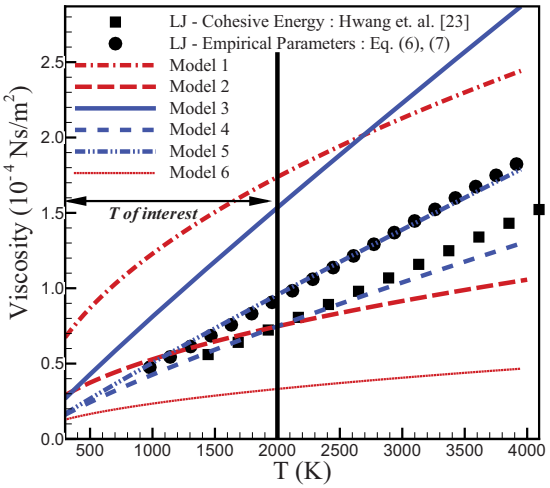

FIG. 1. (Color online) Comparison of variation of viscosity as a function of temperature for two Lennard-Jones potential models and various VHS and HS models used in previous computational studies of atomic copper vapor.

$$\epsilon = 0.281 \text{ eV}.$$

The variation in viscosity as a function of temperature for a gas can be obtained by applying the kinetic theory expressions for transport coefficients based on a prescribed intermolecular potential. The two LJ potential parameters are used to calculate the variation in viscosity as a function of temperature for copper using the procedure described by Hirschfelder *et al.*[25,26] The coefficient of viscosity μ of a pure component is given by

$$\mu = \frac{5}{8\sigma^2}\sqrt{\frac{mkT}{4\pi}}\frac{V}{W^{(2)}(2)}, \tag{8}$$

where V and $W^{(2)}(2)$ are functions of kT/ϵ tabulated in Refs. 25 and 26. While LJ potential is a more realistic representation of the interaction between molecules, it is seldom used in DSMC simulations since it requires a significantly higher computational effort when compared to the HS and the VHS molecular models. Figure 1 compares the variation in viscosity as a function of temperature obtained using the LJ potential parameters with the variation obtained using various HS and VHS molecular models that have been used in previous works of DSMC simulations of copper vapor. Models 1–6, the parameters of which are summarized in Table I, are the models that were considered in the DSMC simulations.

TABLE I. Summary of molecular models used in DSMC simulations.

Model No	Model type	d_{ref} (nm)	T_{ref} (K)	α
1	HS	0.234	300	0.000
2	HS	0.357	300	0.000
3	VHS	0.450	300	0.420
4	VHS	0.550	300	0.310
5	VHS	0.570	300	0.420
6	VHS	0.627	2000	0.349

While model 1 has been used by Sahu *et al.*[18] and Thakur *et al.*[19] to define the Kn of their deposition experiments and also by Mukherjee *et al.*[21] to perform DSMC simulations, model 2 has been used by Briehl *et al.*[20] in their Monte Carlo simulation of a cluster aggregation source. Models 4 and 5 lead to good agreement for the variation in viscosity as a function of temperature obtained using the LJ parameters proposed by Hwang *et al.*[23] and the empirical equations, Eqs. (6) and (7), based on boiling point and molar volume, respectively. Fan *et al.* in their work on DSMC simulations of Yttrium[17] discussed the importance of using an accurate molecular model for the DSMC simulations of deposition processes. The reference diameter and viscosity-temperature exponent for various alkali metal vapors are obtained by fitting parameters of the inverse power-law model to reproduce the viscosity dependence on temperature predicted by experiments. It is then assumed that other metals in the same row of the Periodic Table have same parameters for the inverse power-law model for interaction between molecules. This assumption is equivalent to assuming that the metal vapors have the same viscosity-temperature dependence. Based on this analysis, values for the reference diameter of copper and viscosity-temperature exponent are proposed as $d_{ref}=0.6271$ nm and $\omega=0.849$. The reference temperature for these values is $T_{ref}=2000$ K. This model is referred to as model 6 in the current work.

As can be observed, there are various molecular models proposed for the interaction of copper atoms. Here, it should be mentioned that, for vapor flows typically encountered in vacuum technology applications, viscosity is the most important transport property in operation and hence is being considered as the metric for comparing the various molecular models. A highly viscous vapor flow will have high resistance to flow, thereby leading to a reduction in dimensional mass flux at the collector plate location. The comparison in Fig. 1 shows that the molecular models that have been used in various computational works lead to significantly different viscosity dependence on temperature.

III. DSMC SIMULATION PARAMETERS AND FLOW CONDITIONS

In order to compare the results obtained using DSMC simulations, we consider experimental data available[18] for the electron-beam deposition of copper. Only the key aspects of the setup are presented here. The detailed experimental setup with details of the electron gun can be found in Ref. 19.

Figure 2 shows a schematic of the geometry used in our simulations. It should be mentioned that the symmetry of the problem about $Y=0$ and $Z=0$ has been exploited and only one quarter of the computational domain is shown. The dimension of the two-dimensional slit source is 120×6 mm^2. The collector plate on which the deposition was performed is placed at a distance of 390 mm from the two-dimensional slit source. The collector plate extends from $Z=-0.164$ m to $Z=0.164$ m in the Z-direction and from $Y=-0.204$ m to $Y=0.204$ m in the Y-direction. The mass flux in the experi-

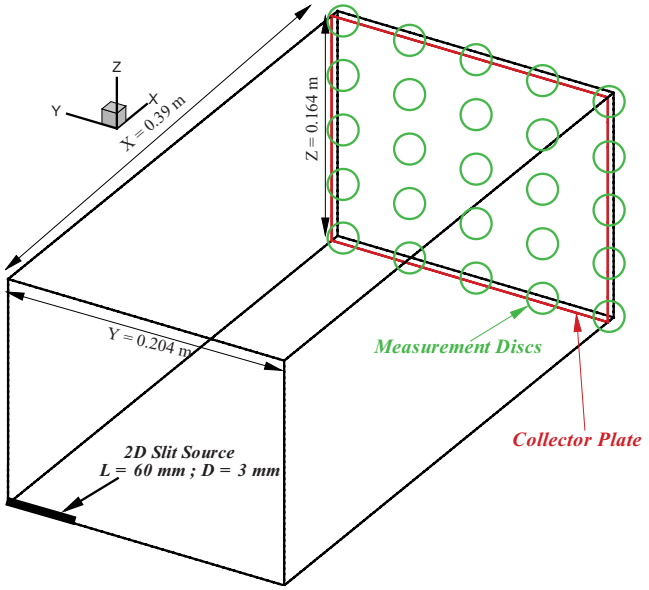

FIG. 2. (Color online) Schematic of the setup used in the experiments and computational domain used in DSMC simulations.

ment was measured by punching out 25 circular disks of diameter of 19 mm at various locations on the collector plate, also shown in the schematic.

The DSMC simulations compute the average mass flux on a given panel based on the number of molecules striking it. In order to ensure that the simulations represent the experimental setup as accurately as possible, the area of the rectangular panels on which the mass fluxes are computed was taken to be the same as the area of the circular disks that were used to measure the mass of copper deposited on them. The number density of the jet at the slit source location corresponds to the saturation number density at the given temperature. For copper, the variation in saturation vapor pressure with temperature is given by

$$\log_{10} P = -\frac{16\,359.806}{T} + 5.816, \tag{9}$$

where P is in atmosphere and T is in kelvins. This is the same relation used by Sahu *et al.*[18] in their experimental work. The mass flux from the source is entirely determined by the temperature of the source and is given by

$$m_f = \tfrac{1}{4} n \bar{c}, \tag{10}$$

where $\bar{c}$ is the average velocity given by

$$\bar{c} = \sqrt{\frac{8RT}{\pi M}}, \tag{11}$$

where M is the atomic weight of copper (0.0635 g/mol).

Mass flux measurements are available[18] at 25 different collector plate locations for four different slit source conditions summarized in Table II.

It should be mentioned that the Knudsen number of a flow depends on the molecular model (reference diameter and viscosity temperature exponent) that is used. The values of Kn

TABLE II. Summary of source conditions listed in Ref. 18.

Case	T (K)	n ($1/m^3$)	Kn
1	1860 ± 10	4.1374×10^{21}	0.166
2	1830 ± 10	3.0172×10^{21}	0.227
3	1760 ± 10	1.3835×10^{21}	0.495
4	1680 ± 10	5.2306×10^{20}	1.310

reported in Table II are obtained using a reference diameter (d_{ref}) of 0.234 nm and a viscosity temperature exponent (ω) of 0.5, which is the same molecular model used by Sahu *et al.* to define the Knudsen number. We compare the experimental data for mass flux at the collector plate locations with those obtained using DSMC simulations and use that to evaluate various molecular models and determine a suitable molecular model for copper-copper intermolecular collisions in DSMC simulations.

The experiments were performed for a given value of the incident power of the electron beam and the resulting slit source temperatures measured using a single color pyrometer[18] are reported. It is also mentioned that the error in temperature is within ± 10 K. However, the published results report that it was not possible to measure the time-averaged temperature of the slit source and the temperature distribution at various locations of the slit source have not been reported. The mass flow rate obtained using the area-averaged temperature will be different from the area-averaged mass flow rate due to the nonlinear relation between temperature and mass flow rate. In order for the simulations to represent a situation as close to the experiments as possible, it is required that the mass flow rates agree well. Therefore, we have the source temperature as a free parameter and perform DSMC simulations for various values of temperature to obtain the desired mass flow rate.

All DSMC simulations presented in this work are performed using one of the six molecular models tabulated in Table I. All molecular models that have been considered in this work are either HS or VHS models mainly because of the computational efficiency of these models as opposed to using a LJ potential to compute intermolecular collisions. The DSMC simulations were performed using the three-dimensional (3D) version of the SMILE (Ref. 27) software system. The ratio of real to simulated molecules was chosen in such a way that it was sufficient to provide good statistics for each of the cases. The numbers of molecules in a cube whose side is equal to the mean free path λ were about 40, 80, 100, and 1000, respectively, for the four cases. Case 4 was simulated with a large number of molecules per λ^3 in order to have good statistics at points away from the lines of symmetry of the rapidly expanding flow.

The timestep was fixed at 1×10^{-6} s for all simulations and it was ensured that this was less than the estimated mean residence time of a molecule in a collision cell. The computational domain was divided into 100, 51, and 41 collision cells in the x, y, and z directions. Each collision cell could

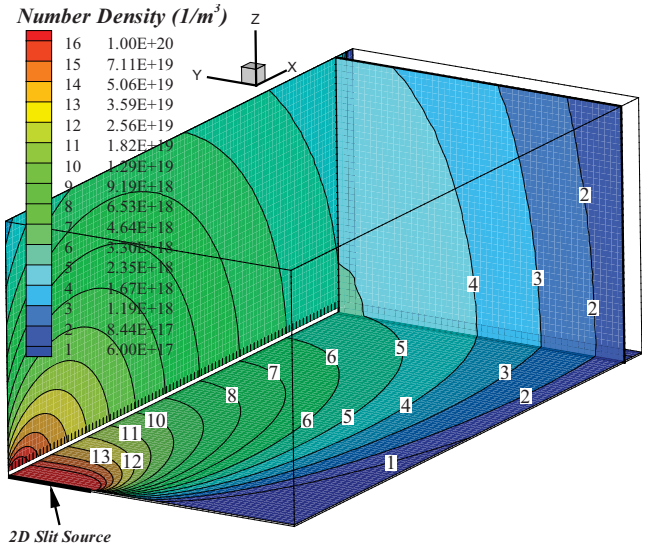

FIG. 3. (Color online) Contours of number density on three slices of the three-dimensional flow field for a source temperature of 1860 K obtained from DSMC simulations using model 4.

further be divided into a maximum of ten level-2 cells in each direction. The number of sampling cells was taken to be same as the number of collision cells. DSMC simulations were performed for various molecular models and source temperatures. In general, varying the molecular model changes the Knudsen number and varying the slit temperature results in different mass flow rates and hence different Knudsen numbers. The slit source was simulated as a jet input with a fixed temperature and the corresponding saturation number density. In calculating the mass flux incident on the collector plates, it was assumed that they had a sticking coefficient of 1.

IV. RESULTS AND DISCUSSION

3D DSMC simulations of metal vapor flow from the e-beam source setup shown in Fig. 2 were performed for various molecular models, source temperatures, and corresponding saturation number densities. The three-dimensional gas flow field computed for a source at a temperature of 1860 K using model 4 is shown in Fig. 3. In order to increase the clarity of information, the density contours are shown only on three slices parallel to the x, y, and z axes, respectively. The flow that is rapidly expanding into vacuum is characterized by strong density gradients. For example, the number density along the $Y=0$, $Z=0$ line drops by three orders of magnitude at a distance of about 0.3 m or 2.5 source lengths from the source.

In order to evaluate the dependence of the dimensional and nondimensional mass fluxes on the molecular model, DSMC simulations performed using the models summarized in Table I were compared with each other. Figure 4 shows comparison of the mass flux and nondimensional contours on the substrate obtained from DSMC simulations using models 2 and 4. Note that the nondimensional mass flux profiles for each case were obtained by nondimensionalizing with respect to the maximum dimensional mass flux for that case. It can be clearly seen that both the mass flux and the nondimensional mass flux contours are significantly different for the two cases. It should be mentioned that, apart from the molecular model, all other parameters including source dimensions, temperature, and number density of the vapor at the source location were the same for the two cases. The temperature of the vapor was fixed at 1860 K with the number density taken as the corresponding saturation number density at that temperature. The corresponding Kn for the two cases were 0.071 and 0.053, respectively. The difference in Kn is due to the use of different molecular models. The trend observed in the results for the dimensional mass flux can be explained by considering the viscosity temperature

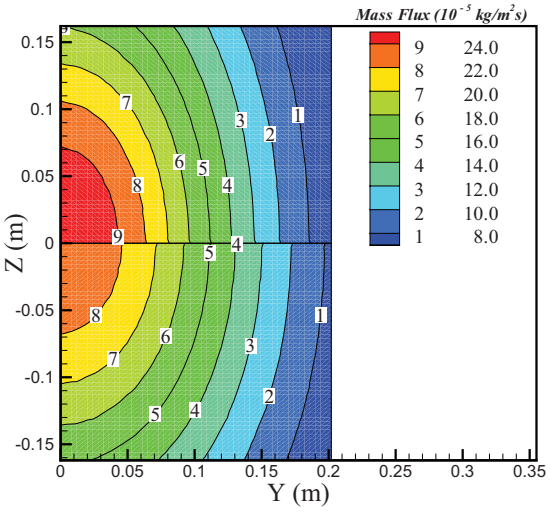

(a) Dimensional mass flux

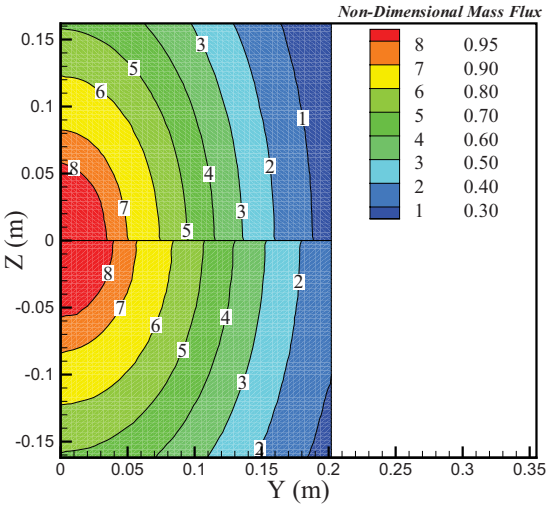

(b) Non-dimensional mass flux

FIG. 4. (Color online) Contours of dimensional and nondimensional mass fluxes on the collector plate for a slit source temperature of 1860 K obtained from DSMC simulations using two different molecular models. Top: model 4; bottom: model 2.

TABLE III. Summary of source conditions used in DSMC simulations for case 1.

Model	T (K)	n ($1/m^3$)	Kn
1	1947	9.7701×10^{21}	0.070
2	1862	4.2239×10^{21}	0.070
3	1893	5.7866×10^{21}	0.069
4	1832	3.0824×10^{21}	0.071
5	1845	3.5378×10^{21}	0.070
6	1755	1.3054×10^{21}	0.070

TABLE V. Summary of source conditions used in DSMC simulations for case 3.

Model	T (K)	n ($1/m^3$)	Kn
1	1857	4.0107×10^{21}	0.171
2	1779	1.7203×10^{21}	0.171
3	1805	2.300×10^{21}	0.171
4	1752	1.2604×10^{21}	0.170
5	1763	1.4324×10^{21}	0.170
6	1681	5.2976×10^{20}	0.171

dependence of the two models considered. Figure 1 shows that model 4 has a lower value of viscosity than model 2 for all temperatures less than 1860 K. The lower value of viscosity leads to lower resistance to the flow, thereby leading to a higher dimensional mass flux as observed in Fig. 4(a).

As explained earlier, the DSMC simulations had two free parameters that could be varied: slit source temperature and molecular model for copper-copper intermolecular collisions. The various sources of uncertainty in measuring the mass fluxes have also been listed[18] and estimated to contribute to an overall uncertainty of $\pm5\%$ in the measured fluxes. DSMC simulations can be assumed to lead to a good prediction of the measured fluxes only if the dimensional mass fluxes agree with the experiments. It is not sufficient if the nondimensional mass flux, obtained from DSMC simulations, agrees with the nondimensional mass flux obtained from the experiments. The DSMC model used by Mukherjee *et al.*[21] to validate similar deposition experiments of copper using two-dimensional slit sources compares only nondimensional quantities which will lead to good agreement as long as the Knudsen number (Kn) of the simulations and experiments agree. As mentioned earlier, the temperature of the slit source is a free parameter in the DSMC simulations and was chosen in such a way that the Kn of all the DSMC simulations considered for a given case were the same. Agreement between the nondimensional mass flux profiles, and hence Kn, of the experiment and the corresponding simulation is a fundamental requirement for possible agreement between the dimensional mass fluxes. It is ensured that all simulations that are performed satisfy this fundamental requirement. The Kn that a given experiment case corresponds to, was chosen by performing a number of DSMC simulations for various Kn, and comparing the nondimensional mass flux profiles obtained from the simulations with those obtained from the experiments. A given deposition experiment corresponds to a Kn if there is good agreement between the nondimensional mass flux profiles obtained from the experiment and the DSMC simulation performed at that Kn. The source conditions, T and n, and the corresponding Kn used for simulation of each of the cases for various molecular models are summarized in Tables III–VI.

Figure 5 shows the comparison of dimensional and nondimensional mass flux at various locations on the collector plate for the experiments and DSMC simulations performed using different molecular models corresponding to case 1. For case 1, the Kn of the simulations shown is approximately 0.069. This can be clearly seen in the comparison of the nondimensional mass flux profiles in which the profiles for the various DSMC simulations and the experiment agree extremely well. However, the dimensional mass flux profiles for the various DSMC simulations are significantly different and only the DSMC simulation performed using molecular model 3 agrees well with the experiments. The maximum errors between the measured mass fluxes and those predicted from DSMC simulations were 72.2%, 32.0%, 7.8%, 51.1%, 44.2%, and 79.8% for models 1–6, respectively. However, the maximum errors for the nondimensional mass flux were 4.0%, 4.2%, 6.1%, 4.5%, 5.5%, and 4.9%, respectively, reiterating the fact that nondimensional parameters are functions only of the Kn. For model 3, the maximum error in dimensional mass flux mentioned above was in one of the collector plates corresponding to the $Y=0.2$ m, that is, farthest away from the source. The average error was 3.1%, less than the 5% uncertainty in the experimental measurements.

TABLE IV. Summary of source conditions used in DSMC simulations for case 2.

Model	T (K)	n ($1/m^3$)	Kn
1	1912	6.9818×10^{21}	0.098
2	1829	2.9850×10^{21}	0.099
3	1858	4.0526×10^{21}	0.098
4	1801	2.2008×10^{21}	0.098
5	1813	2.5109×10^{21}	0.098
6	1726	9.2544×10^{20}	0.098

TABLE VI. Summary of source conditions used in DSMC simulations for case 4.

Model	T (K)	n ($1/m^3$)	Kn
1	1734	1.0187×10^{21}	0.672
2	1666	4.3687×10^{20}	0.674
3	1686	5.6449×10^{20}	0.678
4	1641	3.1428×10^{20}	0.668
5	1650	3.5426×10^{20}	0.667
6	1578	1.3071×10^{20}	0.672

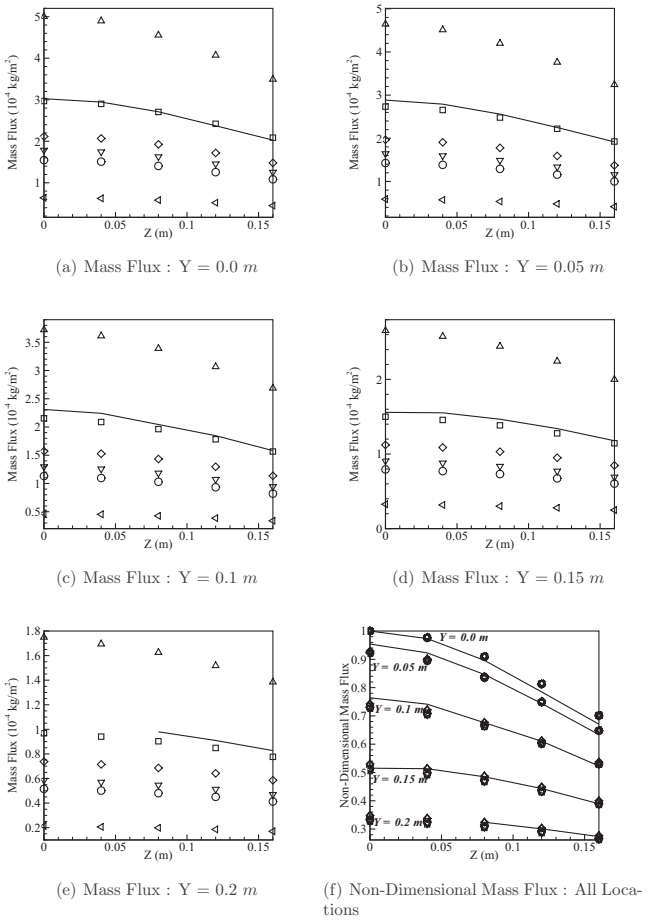

(a) Mass Flux : Y = 0.0 m (b) Mass Flux : Y = 0.05 m

(c) Mass Flux : Y = 0.1 m (d) Mass Flux : Y = 0.15 m

(e) Mass Flux : Y = 0.2 m (f) Non-Dimensional Mass Flux : All Locations

FIG. 5. Comparison of DSMC simulations and experiments for case 1. (△) model 1; (◇) model 2; (□) model 3; (○) model 4; (▽) model 5; (◁) model 6; (solid line) measurements.

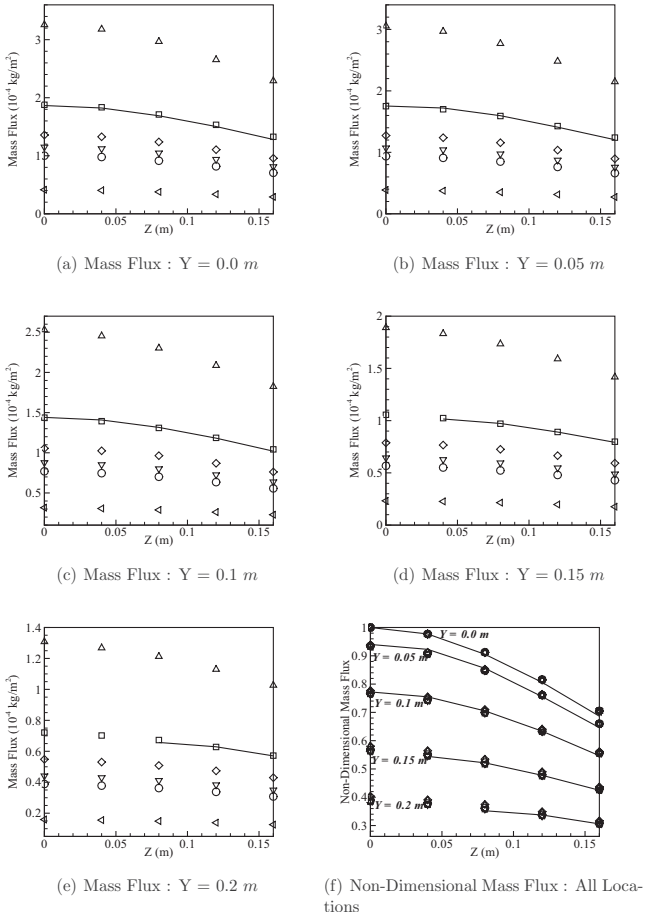

(a) Mass Flux : Y = 0.0 m (b) Mass Flux : Y = 0.05 m

(c) Mass Flux : Y = 0.1 m (d) Mass Flux : Y = 0.15 m

(e) Mass Flux : Y = 0.2 m (f) Non-Dimensional Mass Flux : All Locations

FIG. 6. Comparison of DSMC simulations and experiments for case 2. (△) model 1; (◇) model 2; (□) model 3; (○) model 4; (▽) model 5; (◁) model 6; (solid line) measurements.

A similar comparison of dimensional and nondimensional mass fluxes is shown for case 2 in Fig. 6. The source temperatures for the DSMC simulations performed using various molecular models were chosen in such a way that they all correspond to a Kn of about 0.098. As mentioned earlier, this value of the Kn was estimated by comparing the nondimensional mass flux profiles obtained from experiments with around 20 DSMC simulations performed at various Kn. The trend for case 2 is very similar to case 1 with model 1 overpredicting the dimensional mass flux and models 2, 4, 5, and 6 under predicting it. On the other hand, the DSMC simulation performed using molecular model 3 once again leads to very good agreement for not just the nondimensional mass fluxes but also the dimensional mass fluxes at the collector plate location. The maximum errors between the measured mass fluxes and those predicted from DSMC simulations were 84.6%, 28.1%, 3.6%, 39.5%, 47.1%, and 78.2% for models 1–6, respectively. However, the maximum errors for the nondimensional mass flux were 6.3%, 4.2%, 2.9%, 2.9%, 2.7%, and 2.2%, respectively.

Figures 7 and 8 show results for cases 3 and 4. The Kn used for the DSMC simulations were 0.17 and 0.67, respectively. These cases show a similar trend with model 3 leading to reasonably good agreement for both dimensional and nondimensional mass fluxes except for the collector plates corresponding to Y=0.20 m, located farthest from the slit source. For case 3, the maximum errors between the measured mass fluxes and those predicted from DSMC simulations were 122.5%, 24.9%, 23.2%, 45.1%, 37.7%, and 76% for models 1–6, respectively. The maximum errors for the nondimensional mass flux were 23.1%, 23.0%, 20.7%, 21.0%, 20.1%, and 18.4%, respectively. The nondimensional mass flux errors reported are all at the collector plate location farthest from the source. As can be observed from the nondimensional mass flux profiles in Fig. 7(f), the agreement for the nondimensional mass flux at the collector plate row farthest from the source is not very good. It should be mentioned that the high maximum error in the dimensional mass flux obtained for DSMC simulations using model 3 is in one of the collector plates located the farthest from the source. The average error is 8.7%, a little higher than the uncertainty reported in the experiments. For case 4, the maximum errors between the measured mass fluxes and those predicted from DSMC simulations were 105.6%, 22.2%, 10.9%, 44.6%, 38.2%, and 77.5% for models 1–6, respectively. The maximum errors for the nondimensional mass flux were 11.9%, 11.6%, 11.4%, 10.6%, 12.6% and 11.7%, respectively. For case 4, the average error in dimensional mass flux using

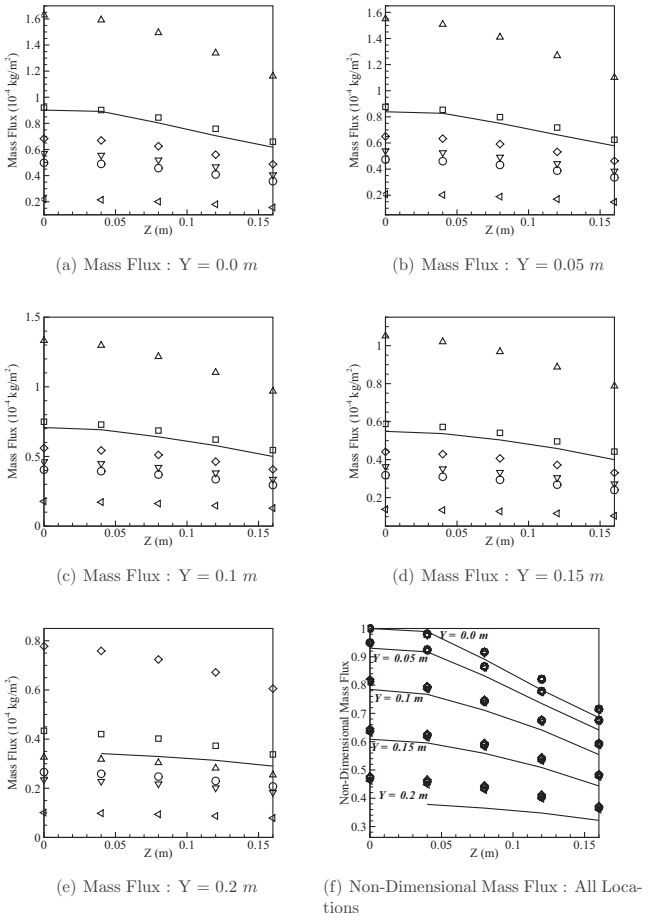

(a) Mass Flux : Y = 0.0 m (b) Mass Flux : Y = 0.05 m

(c) Mass Flux : Y = 0.1 m (d) Mass Flux : Y = 0.15 m

(e) Mass Flux : Y = 0.2 m (f) Non-Dimensional Mass Flux : All Locations

FIG. 7. Comparison of DSMC simulations and experiments for case 3. (△) model 1; (◇) model 2; (□) model 3; (○) model 4; (▽) model 5; (◁) model 6; (solid line) measurements.

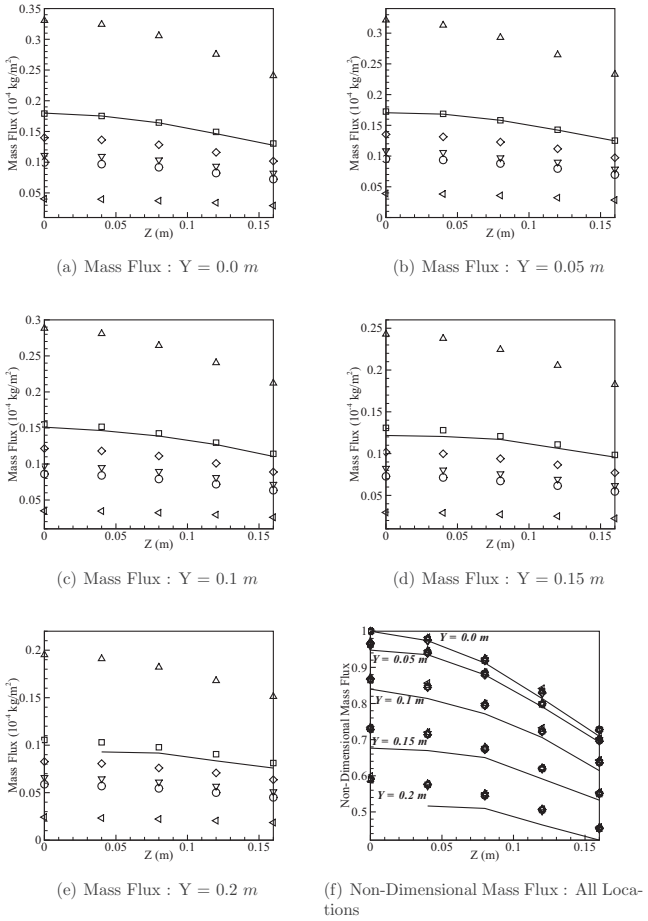

(a) Mass Flux : Y = 0.0 m (b) Mass Flux : Y = 0.05 m

(c) Mass Flux : Y = 0.1 m (d) Mass Flux : Y = 0.15 m

(e) Mass Flux : Y = 0.2 m (f) Non-Dimensional Mass Flux : All Locations

FIG. 8. Comparison of DSMC simulations and experiments for case 4. (△) model 1; (◇) model 2; (□) model 3; (○) model 4; (V) model 5; (◁) model 6; (solid line) measurements.

model 3 is 3.2%. The disagreement at collector plates far away from the source, even for the nondimensional mass flux profiles, could be due to various reasons including possible errors in measuring small values of mass flux at these locations and these collector plates contribute the maximum to the average errors reported, and as can be observed in Figs. 7 and 8, the agreement is very good for collector plates closer to the source.

V. CONCLUSIONS

DSMC simulations were performed for the e-beam assisted deposition of copper thin films with a goal of determining a molecular model for copper vapor. Predictions for the nondimensional and dimensional mass fluxes obtained using various VHS models have been compared with published experimental data. The comparisons have been carried out for different deposition source temperatures and at multiple locations on deposition samples.

It has been established that the VHS models formulated to reproduce the viscosity-temperature dependence predicted by the Lennard-Jones potential with parameters available in the literature do not agree well with measurements. This can be attributed to the fact that the LJ parameters are based on solid and liquid phase measurements and hence may not predict the vapor-phase viscosity variation accurately.

However, a VHS model with a higher effective viscosity than the Lennard-Jones models leads to a very good agreement, within 5%, with measurements for both dimensional and nondimensional fluxes. The parameters of the model are given by a reference diameter d_{ref}=0.45 nm, an exponent α=0.42, and a reference temperature of T_{ref}=300 K. The VHS molecular model determined for copper can be used for design of vacuum thin-film deposition systems allowing for accurate prediction of growth rates as well as uniformity and microstructure.

[1]D. L. Smith, *Thin-Film Deposition: Principles and Practice* (McGraw-Hill, New York, 1995).
[2]J. J. Allen, *Micro-Electro Mechanical System Design* (CRC, Boca Raton, FL, 2005).
[3]B. Bhushan, *Springer Handbook of Nanotechnology* (Springer, New York, 2006).
[4]R. Bakish, *Introduction to Electron Beam Technology* (Wiley, New York, 1962).
[5]R. F. C. Farrow, *Molecular Beam Epitaxy: Applications to Key Materials* (Noyes, Park Ridge, NJ, 1995).
[6]J. H. Park and T. S. Sudarshan, *Chemical Vapor Deposition* (ASM International, Metals Park, OH, 2001).
[7]T. Itoh, *Ion Beam Assisted Film Growth* (Elsevier, Amsterdam, 1989).
[8]J. Singh, F. Quli, D. Wolfe, J. Schriempf, and J. Singh, Surf. Eng. **1**, 59

(1999).
[9]J. Singh and D. Wolfe, J. Mater. Sci. **40**, 1 (2005).
[10]T. Zhang, S. Boyd, A. Vijayaraghavan, and D. Dornfeld, Proceedings of the 2006 IEEE International Symposium on Electronics and Environment, 2006 (unpublished).
[11]M. Knudsen, *Kinetic Theory of Gases—Some Modern Aspects* Methuen's Monographs on Physical Subjects (Wiley, London, 1952).
[12]G. A. Bird, *Molecular Gas Dynamics and the Direct Simulation of Gas Flows* (Oxford University Press, New York, 1994).
[13]G. Chen and I. D. Boyd, *20th International Symposium of Rarefied Gas Dynamics* (Peking University, Beijing, 1996).
[14]G. Chen, I. D. Boyd, S. E. Roadman, and J. R. Engstrom, J. Vac. Sci. Technol. A **16**, 689 (1998).
[15]G. Ghen and I. D. Boyd, Mater. Sci. Semicond. Process. **1**, 141 (1998).
[16]J. Balakrishnan, I. D. Boyd, and D. G. Braun, J. Vac. Sci. Technol. A **18**, 907 (2000).
[17]J. Fan, I. D. Boyd, and C. Shelton, J. Vac. Sci. Technol. A **18**, 2937 (2000).
[18]G. K. Sahu and K. B. Thakur, Vacuum **81**, 77 (2006).
[19]K. B. Thakur and G. K. Sahu, J. Phys. D **35**, 1812 (2002).
[20]B. Briehl and H. M. Urbassek, J. Vac. Sci. Technol. A **17**, 256 (1999).
[21]J. Mukherjee, L. Gantayet, and K. Thakur, Vacuum **83**, 828 (2009).
[22]M. Kogan, *Rarefied Gas Dynamics* (Plenum, New York, 1969).
[23]H. J. Hwang, O. K. Kwon, and J. W. Kang, Solid State Commun. **129**, 687 (2004).
[24]R. B. Bird, W. E. Stewart, and E. N. Lightfoot, *Transport Phenomena* (Wiley, New York, 2001).
[25]J. O. Hirschfelder, R. B. Bird, and E. L. Spotz, J. Chem. Phys. **16**, 968 (1948).
[26]J. O. Hirschfelder, C. F. Curtiss, and R. B. Bird, *Molecular Theory of Gases and Liquids* (Wiley, New York, 1954).
[27]M. S. Ivanov, A. V. Kashkovsky, S. F. Gimelshein, G. N. Markelov, A. A. Alexeenko, Ye. A. Bondar, G. A. Zhukova, S. B. Nikiforov, and P. V. Vaschenkov, *25th International Symposium on Rarefied Gas Dynamics* (Russian Academy of Sciences, St. Petersburg, Russia, 2006), pp. 539–544.